

# Oxygen vacancies dynamics in redox-based interfaces: Tailoring the memristive response

Cristian Ferreyra<sup>1</sup>, Wilson Román Acevedo<sup>1</sup>, Ralph Gay<sup>2</sup>, Diego Rubi<sup>1</sup>

<sup>1</sup>*GIyA and INN, CNEA, Av. Gral Paz 1499 (1650), San Martín, Buenos Aires, Argentina.*

<sup>2</sup>*CIC nanoGUNE, Tolosa Hiribidea 76, 20018 Donostia-San Sebastián, Spain.*

María José Sánchez

*INN, Centro Atómico Bariloche and Instituto Balseiro, 8400 San Carlos de Bariloche, Argentina.*

(Dated: March 17, 2022)

Redox-based memristive devices are among the alternatives for the next generation of non volatile memories, but also candidates to emulate the behavior of synapses in neuromorphic computing devices. It is nowadays well established that the motion of oxygen vacancies (OV) at the nanoscale is the key mechanism to reversibly switch metal/insulator/metal structures from insulating to conducting, i.e. to accomplish the resistive switching effect.

The control of OV dynamics has a direct effect on the resistance changes, and therefore on different figures of memristive devices, such as switching speed, retention, endurance or energy consumption. Advances in this direction demand not only experimental techniques that allow for measurements of OV dynamics, but also of theoretical studies that shed light on the involved mechanisms. Along this goal, we analyze the OV dynamics in redox interfaces formed when an oxidizable metallic electrode is in contact with the insulating oxide. We show how the transfer of OV can be manipulated by using different electrical stimuli protocols to optimize device figures such as the ON/OFF ratio or the energy dissipation linked to the writing process. Analytical expressions for attained resistance values, including the high and low resistance states are derived in terms of total transferred OV in a nanoscale region of the interface. Our predictions are validated with experiments performed in Ti/La<sub>1/3</sub>Ca<sub>2/3</sub>MnO<sub>3</sub> redox memristive devices.

## I. INTRODUCTION

Resistance random access memory (ReRAM) devices have emerged as one of the main alternatives to current flash memory technologies. Besides their potential application in the field of non-volatile memories, they have been also tested as logic devices<sup>1</sup>, and more recently, in the emergent field of neuromorphics<sup>2</sup>.

The physical phenomenon behind ReRAMs is the so-called Resistive Switching (RS) effect, which is the reversible and non-volatile change of the resistance of a metal/insulator/metal structure upon the application of electrical stimulus<sup>3–5</sup>.

The RS has been ubiquitously found in simple and complex oxides based devices and, in particular, in manganese oxides known as manganites<sup>6</sup>. In these compounds the switching is usually of bipolar type, which requires opposite polarities for the electrical stimuli to achieve both the SET (high to low resistance, HR→LR) and RESET (low to high resistance, LR → HR) transitions.

It was recently shown that when oxidizable metals such as Ti or Al are used as electrodes, a thin oxide layer (TiO<sub>x</sub> or AlO<sub>x</sub>) is naturally formed at the interface between the metal electrode and the insulating oxide. In particular, in the case of Ti/LCMO(PCMO)<sup>7</sup>, the manganite is spontaneously reduced after the deposition of Ti. This results in a mixed interface TiO<sub>x</sub> / LCMO<sub>3–x</sub> (PCMO<sub>3–x</sub>) in which the TiO<sub>x</sub> layer behaves as a n-type semiconductor and is in contact with the p-type reduced manganite, forming a n-p diode. In these samples, the

RS behavior has been related to a redox process involving the transfer of oxygen ions through the n-p layer<sup>9,10</sup>, while the other interfaces behave as ohmic<sup>11,12</sup>. We have recently shown that the redox process is activated after the n-p diode is polarized in direct mode, or in inverse mode above breakdown<sup>13</sup>.

The Voltage Enhanced Oxygen Vacancies drift (VEOV) model was originally developed to explain the RS behaviour in single manganites samples<sup>14</sup> and it was further extended to analyse binary oxides based devices<sup>15</sup>. It has been extensively tested in RS experiments with several devices of the type M1/Oxide/M2, with M1 and M2 metallic electrodes (like Pt, Au, Cu, Al), and oxides compounds ranging from manganites (PCMO, LCMO) and cuprates (YBCO), to binary oxides like TiO<sub>2</sub><sup>14–19</sup>.

Recently, the VEOV model has been also adapted to mimic the RS behavior in Ti/LCMO/Pt samples, where the mixed TiO<sub>x</sub>/LCMO<sub>3–x</sub> interface dominates the memristive behavior of the device as a consequence of the redox process already described<sup>13</sup>.

With quite a few exceptions<sup>18,20,21</sup> most of the theoretical studies disregard the connection between OV dynamics and the manipulation of the attained resistance states. The ability to reversibly control the concentration and profile of OV should have a straightforward impact on the resistance changes, allowing the improvement of the performance of practical devices. This can lead, for example, to the optimization of switching speeds or to the minimization of the energy consumption for the writing process. Advances in this direction demand not only

experimental techniques that allow for measurements of OV dynamics<sup>23–25</sup>, but also of theoretical studies that shed light on the involved mechanisms. Along this goal, here we perform a systematic analysis of the dynamics of OV in redox interfaces, and their response to different protocols and stimuli. We show the modelling to predict how the electrical stimuli can be manipulated to control OV dynamics and optimize memristive figures such the ON/OFF ratio or the energy consumption linked to the RESET process.

In addition, we derive analytical expressions for the attained resistance values in terms of the total amount of OV transferred along the interface and as a function of the applied voltage. This enables the reconstruction of the R vs V resistance hysteresis switching loops (HSL).

Our predictions are validated with experiments performed on the Ti/LCMO interface, demonstrating the capability of this kind of simulations to understand the physics related to redox memristive processes, paving the way to optimize the electrical response of practical devices.

## II. THE VEOV MODEL REVISITED FOR MIXED REDOX INTERFACES

In order to be self contained and to clarify notation, we describe here the main assumptions and equations of the VEOV<sup>14,15</sup> migration model here adapted for the study of RS in the mixed interface  $\text{TiO}_x/\text{LCMO}_{3-x}$ <sup>13</sup>.

The interface is the active region for the RS behavior, and it is modelled as a 1D chain of  $N = Nl + Nr$  total sites, where  $Nl$  sites are associated to the  $\text{TiO}_x$  layer and  $Nr$  sites to the  $\text{LCMO}_{3-x}$ , respectively. The links physically represent small domains of nanoscopic dimensions in both sub-oxides with an initial OV concentration that might correspond to the pristine state (PS).

We characterize each domain  $i$  along the chain by its resistivity  $\rho_i$  which is a function of the local OV density,  $\delta_i$ . An universal feature of oxides is that their resistivity is dramatically affected by the precise oxygen stoichiometry. LCMO is a complex oxide that behaves as a p-type semiconductor in which OV disrupt the Mn-O-Mn bonds with the concomitant increment of the resistivity. On the other hand,  $\text{TiO}_x$ , behave as n-type semiconductor in which oxygen vacancies increment its conductivity. As a consequence, we adopt for the first  $Nl$  domains associated to the  $\text{TiO}_x$  the (most simple) relation between resistivity and OV density:

$$\rho_i^l = \rho_0^l - A_i \delta_i. \quad (1)$$

where we define  $\rho_0^l$  as the residual resistivity of the left layer for negligible OV concentration ( $\delta_i = 0$ ). As the model description is given in terms of OV, we conceive the  $\text{TiO}_x$  as an OV doped  $\text{TiO}_2$  and therefore  $\rho_0^l$  corresponds to the resistivity of  $\text{TiO}_2$ , (i.e.  $x \sim 2$ ).

On the other hand, as the resistivity of the  $\text{LCMO}_{3-x}$  layer increases due to the presence of OV<sup>22</sup> we define for sites  $i = Nl + 1, N$ :

$$\rho_i^r = \rho_0^r + B_i \delta_i, \quad (2)$$

being  $\rho_0^r$  the residual resistivity of the stoichiometric LCMO. The coefficients,  $A_i$  and  $B_i$  are specific of each layer (oxide) and can be taken either as constants or smoothly dependent on the site position, without affecting the qualitative behaviour of the simulated results.

The total resistance along the interface is computed as  $R = c \sum_{i=1}^N \rho_i$ , with the scale factor taken for simplicity  $c \equiv 1$ . Following Eqs.(1,2) we obtain

$$\begin{aligned} R &= \sum_{i=1}^{Nl} \rho_i^l + \sum_{i=Nl+1}^N \rho_i^r, \\ &= R_s - \sum_{i=1}^{Nl} A_i \delta_i + \sum_{i=Nl+1}^N B_i \delta_i, \end{aligned} \quad (3)$$

with  $R_s \equiv Nl \rho_0^l + Nr \rho_0^r$  the residual resistance of the interface, which is assumed known.

Given an external stimulus (either a current  $I(t)$  or a voltage  $V(t)$ ) applied to the interface at time  $t$ , the OV density at site  $i$  is updated for each simulation step according to the rate probability  $p_{ij} = \delta_i(1 - \delta_j) \exp(-V_\alpha + \Delta V_i)$ , for a transfer from site  $i$  to a nearest neighbor  $j = i \pm 1$ . Notice that  $p_{ij}$  is proportional to the OV present at site  $i$ , and to the available concentration at the neighbour site  $j$ <sup>14</sup>. In order to restrict the dynamics of OV to the interface region, we take  $p_{01} = p_{10} = p_{NN+1} = p_{N+1N} = 0$ .

In the Arrhenius factor  $\exp(-V_\alpha + \Delta V_i)$ ,  $\Delta V_i$  is the local potential drop at site  $i$  defined as  $\Delta V_i(t) = V_i(t) - V_{i-1}(t)$  with  $V_i(t) = I(t)\rho_i = V(t)\rho_i/R$ . We denote  $V_\alpha$  the activation energy for vacancy diffusion in the absence of external stimulus. All the energy scales are taken in units of the thermal energy  $k_B T$  and we consider  $V_\alpha = V_A$ , for sites in the left layer ( $\text{TiO}_x$ ), and  $V_\alpha = V_B$  for those in the right layer ( $\text{LCMO}_{3-x}$ ).

The numerical implementation starts with the input of the initial OV profile along the interface,  $\delta_i(0), \forall i = 1..N$ . Different electrical protocols can be employed. According to standard RS experiments, we chose the stimulus  $V(t)$  as a linear ramp following the cycle  $0 \rightarrow V_{m1} \rightarrow -V_{m2} \rightarrow 0$  a.u. At each simulation time step  $t_k$  we compute the local voltage profile  $V_i(t_k)$  and the local voltage drops  $\Delta V_i(t_k)$ . Employing the probability rates  $p_{ij}$  we obtain the transfers between nearest neighboring sites. Afterwards the values  $\delta_i(t_k)$  are updated to a new set of densities  $\delta_i(t_{k+1})$ , with which we compute, at time  $t_{k+1}$ , the local resistivities  $\rho_i(t_{k+1})$ , the local voltage drops under the applied voltage  $V(t_{k+1})$ , and finally from Eq.(3) the total resistance  $R(t_{k+1})$ , to start the next simulation step at  $t_{k+1}$ .

The initial configuration of OV in the pristine state (PS) has been taken consistently with the experimentally

reported (low resistance) initial state<sup>9,13</sup>, for which the non-stoichiometric  $\text{TiO}_x$  layer ( $x < 2$ ) contributes with a significant conductivity. The partial oxidation of Ti layer is at expenses of the reduction of the thin LCMO layer that becomes  $\text{LCMO}_{3-x}$ . This redox process has been clearly identified through spectroscopic characterization by the Jülich group in Ref.9. Taking into account this scenario, the initial OV density in the  $\text{TiO}_x$  is such to grant an appreciable conductivity to this layer. Additionally, as the resistivity of the  $\text{LCMO}_{3-x}$  increases due to the presence of OV, we chose an OV profile for the PS that matches these requirements and compatible with the (low resistance) initial state of the complete interface (see Fig.1(b)).

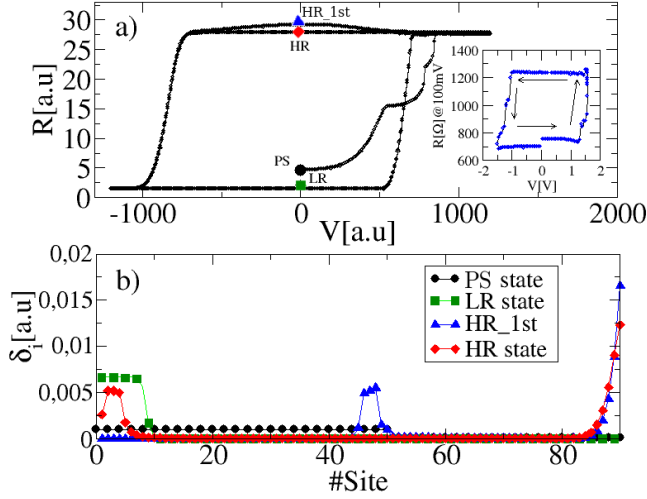


FIG. 1: a)  $R$  vs  $V$  (HSL) obtained within the VEOV model for the 1st and 2nd cycles of the voltage protocol  $0 \rightarrow V_{m1} \rightarrow -V_{m2} \rightarrow 0$ . In the simulations we take  $V_{m1} = |V_{m2}| = 1200$  a.u. and  $N = 90, Nl = 50, A = 750, B = 50, V_A = 8.5, V_B = 6$ . The two latter values are chosen following Refs.15 and 26, which report OV diffusions barrier for  $\text{TiO}_x$  (up to 2.5 eV) and LCMO ( $\sim 1.3$  eV). Inset: Experimental HSL for a single cycle of the voltage protocol, with  $V_{m1} = |V_{m2}| = 1.8$  V. The arrows indicate the circulation. b) OV density profiles,  $\delta_i$ , for different resistance states indicated respectively in the HSL's of panel a). See text for details.

In Fig.1(a) we show a typical  $R$  vs  $V$  Hysteresis Switching Loop (HSL), obtained from the numerical simulations with the VEOV model for a symmetric voltage ramp i.e.  $V_{m1} = |V_{m2}|$ . Two consecutive cycles are considered in order to show the initial resistance (correspondent to  $t=0, V=0$ ) of the PS state, together with the slightly erratic response of the beginning of the 1st voltage cycle.

In the experiments reported in Refs.9 and 13, the RESET process takes place for positive stimulus and it is related to the transfer of OV (positive ions) from the  $\text{TiO}_x$  layer to the  $\text{LCMO}_{3-x}$  layer, the first becoming

nearly stoichiometric ( $x \sim 2$ ) and thus highly resistive. At the same time, OV at the  $\text{LCMO}_{3-x}$  contribute to increase the resistance. In Fig.1(b), the OV profile associated to the HR state of the 1st HSL is shown, in complete agreement with the described behaviour.

The SET transition takes place for negative stimulus, when the interface returns to a LR state. The associated OV profile shown in Fig.1(b) corresponds to the LR state after the completion of the 1st HSL. In this case OV accumulate at the left side of the left interface, while for initial PS, which indeed has a higher resistance value, the density of OV is constant. Besides the initial erratic behavior of the 1st HSL, the HR and LR states associated to the next cycles of the voltage protocol become highly repetitive and stable. As an example, we also show in Fig.1(b) the OV configuration for the HR state of the 2nd HSL.

The inset of Fig.1(a) shows an experimental HSL recorded for the Ti/LCMO interface, for a complete cycle of the applied voltage protocol. The similarity between the simulated and experimental HSL's is remarkable, demonstrating the ability of the VEOV model to collect the physics of the memristive effect. Notice that as the amount of transferred OV is controlled by the amplitudes of the electrical stimuli, different experimental HSL can be obtained by tuning the voltage (or current) excursions, as it was already discussed in Ref.13, where details of the device fabrication can be also found.

### III. RESISTANCE IN TERMS OF TRANSFERRED OXYGEN VACANCIES

In this section we advance a step further and derive analytical expressions for the resistance values cast in terms of the transferred OV as a function of the applied stimulus.

As in typical experiments, the external electrical stress can be either voltage  $V(t)$  or current  $I(t)$ . For the sake of simplicity we consider voltage controlled experiments following the aforementioned protocol, but the following reasoning will be valid when the stimulus is  $I(t)$ .

We start from the initial state, correspondent to the OV configuration depicted in Fig.1 b), consistent with the PS. Taking into account Eq.(3) we write

$$R(0) = R_s - A al_0 + B ar_0, \quad (4)$$

where  $R_s$  has been previously defined and we here denote the left and right initial **areas** (total number of OV), as  $al_0 \equiv \sum_{i=1}^{Nl} \delta_{i,0}$  and  $ar_0 \equiv \sum_{i=Nl+1}^N \delta_{i,0}$ , respectively, with  $\delta_i(0) \equiv \delta_{i,0}$ , the OV density at site  $i$  for the initial state.

Positive voltages  $0 < V \leq V_{m1}$ , move OV (as positive ions) from the left layer of the interface ( $\text{TiO}_x$ ) to the right layer ( $\text{LCMO}_{3-x}$ ), as we have already described. For each value of  $V(t) > 0$  it is possible to compute the number of transferred vacancies  $a^+(V(t))$ . Taking into account the conservation of the total number of OV, we

define  $al^+(V) = al_0 - a^+(V)$  and  $ar^+(V) = ar_0 + a^+(V)$ . In this way we can write:

$$\begin{aligned} R^+(V) &= R_s - A al^+(V) + B ar^+(V) \\ &= R(0) + (A + B) a^+(V), \end{aligned} \quad (5)$$

showing that the resistance  $R^+(V)$  for positive voltages  $V(t)$  is determined by the transferred area  $a^+(V)$  and sample specific parameters. As  $a^+$  increases,  $R^+$  attains higher values and thus it might be expected that for a sufficiently strong voltage  $V_R \leq V_{m1}$ , the RESET transition to the HR state takes places, i.e.  $R^+(V_R) \equiv \text{HR}$ .

In the next section we will study the OV transfer process in order to analyse different scenarios for the RESET transition. An important issue that will be addressed is whether the RESET takes place for  $a^+(V_R) = al_0$  (complete transfer of the initial number of OV), or alternatively for  $a^+(V_R) < al_0$ .

For negative voltages, OV move from the right to left side of the interface. Defining  $a^-(V)$  as the net transferred area for a (negative) voltage  $|V| \leq V_{m2}$ , we can write  $al^-(V) = al_0 - a^+(V_R) + a^-(V)$  and  $ar^-(V) = ar_0 + a^+(V_R) - a^-(V)$ , for the left and right interfaces, respectively. For simplicity we have assumed that once the RESET transition takes places for positive polarities and until the reversal of the voltage polarity, the transfer of vacancies from the right to the left interface is inhibited. This assumption is consistent with the (almost) flat shape of the HSL experimentally observed for this range of voltages (see inset of Fig.1 a)). Thus we write for  $|V| \leq V_{m2}$ ,

$$\begin{aligned} R^-(V) &= R_s - A al^-(V) + B ar^-(V) \\ &= R_0 + (A + B) \{a^+(V_R) - a^-(V)\}. \end{aligned} \quad (6)$$

In analogy with the previous description, we define the SET transition for a negative voltage  $|V_S| \leq V_{m2}$  with an associated transferred area  $a^-(V_S)$ . Therefore, from Eq.(6), the low resistance LR state is  $R^-(V_S) = R_0 + (A + B) \{a^+(V_R) - a^-(V_S)\} \equiv \text{LR}$ .

We can proceed along for additional cycles of the applied voltage protocol, but as the systematics is essentially the same as the one already detailed, we restrict the explicit description to a single cycle.

From Eqs.(5) and (6) it is possible to reconstruct  $R$  for a complete cycle of  $V(t)$ , i.e. the HSL, once the transferred areas are determined.

Depending on the relation between  $a^+(V_R)$  and  $a^-(V_S)$  different scenarios emerge for the LR state. In those cases where  $a^+(V_R) = a^-(V_S)$ , the attained LR state results identical to the initial one, see Eq.(6). However in other cases where  $a^+(V_R) \leq a^-(V_S)$  the LR  $\leq R_0$ . These responses have been already observed in the experiment of Ref.13 and give rise to close or open HSL after a complete cycle of the voltage excursion.

Besides the formal simplicity of Eqs.(5) and (6), the analytical determination of  $a^+(V)$  and  $a^-(V)$  is not a trivial task. In the following we summarize the main steps followed to obtain  $a^+$ , and refer the readers to the

Appendix for further details. As  $V(t)$  is a known function of the (discretized) elapsed time  $t \equiv \sum_k t_k$ , the total transferred area can be written as  $a^+(t) = \sum_k a^+(t_k)$ . To simplify the notation, we denote  $a_k^+ \equiv a^+(t_k)$ . After a lengthy calculation, we can write (see Appendix):

$$a_k^+ = a_k^{+L} + a_k^{+NL}, \quad (7)$$

where we define the linear and non linear contributions respectively as:

$$\begin{aligned} a_k^{+L} &= C_{Nl} \delta_{Nl}(k) \exp(I(k) \rho_{Nl}(k)) - C_{Nl+1} \delta_{Nl+1}(k) \\ &\quad \exp(-I(k) \rho_{Nl+1}(k)), \\ a_k^{+NL} &= -\delta_{Nl}(k) \delta_{Nl+1}(k) \{ -C_{Nl+1} \exp(-I(k) \rho_{Nl+1}(k)) \\ &\quad + C_{Nl} \exp(I(k) \rho_{Nl}(k)) \}, \end{aligned} \quad (8)$$

with  $I(k) = V(k)/R(k)$ , following the adopted convention.

Notice that in the case of current controlled experiments, in which  $I(k)$  is known, the above equations stress that the transferred area  $a_k^+$  for the time interval  $t_k$  is determined in terms of the density of OV at the **two frontier sites of the interface**, i.e.  $\delta_{Nl}(k)$  and  $\delta_{Nl+1}(k)$ , respectively. This is a nontrivial result, that could be experimentally tested using OV imaging techniques<sup>23</sup> in current controlled experiments, and should contribute to the design of optimized interfaces for RS experiments.

Equation(8) can be further simplified taking into account that the activation energies satisfy  $V_A < V_B$ , which implies  $C_{Nl} \gg C_{Nl+1}$ . Taking into account this approximation, the obtained analytical estimates for  $a_k^+$  (see Eq.(A12)) enable the determination of the transferred areas as a function of the applied stimulus.

In the Appendix, we also derived estimates for  $a_k^-$  (see Eq.(A17)) to compute the transferred area  $a^- = \sum_k a_k^-$  for the case of negative applied stimulus.

To give a concrete example, we consider protocols controlled by the current for which the expressions for  $a^+(I)$  and  $a^-(I)$  acquire its simplest form, due to the fact that  $I(k)$ , the current at each time step  $t_k$ , is known. Figure 2 shows the analytical estimates for  $a^+(I)$  and  $a^-(I)$  obtained for a current loop  $I(t) = 0 \rightarrow I_{m1} \rightarrow -I_{m2} \rightarrow 0$ . Notice that the conversion from transferred areas to resistance values is trivial following equations analogous to Eqs.(5) and (6), for the case of current control experiments. Thus, the analytical reconstruction of the HSL,  $R$  vs  $I$ , in terms of the applied stimulus is fully accomplished. The analytical estimates, that only consider the OV at sites  $Nl$  and  $Nl + 1$ , result almost indistinguishable from the numerical values (see Fig.2) obtained with the VEOV model. In this last case the complete OV profile along the whole interface has to be updated at each simulation step  $t_k$ , which demands an appreciable computational effort.

An important figure of merit is the HR/LR ratio which, from Eqs.(5) and (6), can be expressed as:

$$\frac{RL - R_0}{RH - R_0} = \frac{a^+(V_R) - a^-(V_S)}{a^+(V_R)}, \quad (9)$$



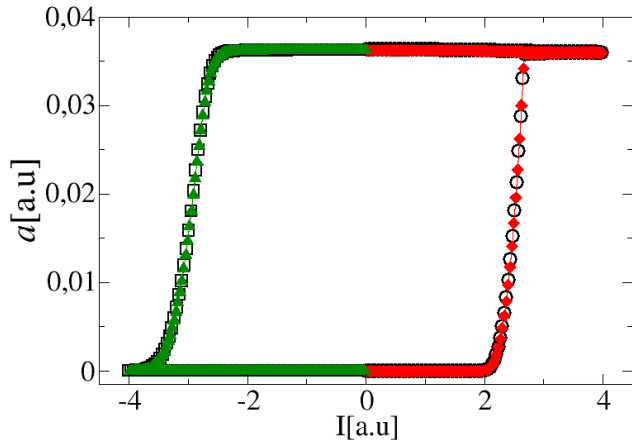


FIG. 2: Transferred area  $a^+(I)$  ( $a^-(I)$ ) for a protocol  $I(t) = 0 \rightarrow I_{m1} \rightarrow 0$  ( $0 \rightarrow -I_{m2} \rightarrow 0$ ). The circles (squares) were obtained following the analytical estimates Eq.(A12)) (Eq.(A17)). The diamond and triangle symbols correspond to the numerical calculations employing the VEOV model simulations. We take  $I_{m1} = I_{m2} = 4a.u$

taking as a reference value  $R_0$ .

To give a further insight into the transfer area process, in the next section we will analyze the dynamics of OV for different electrical protocols. This will allow to determine an optimal stimuli protocol, which shall be confirmed by our experiments on the Ti/LCMO interface.

#### IV. DYNAMICS OF OXYGEN VACANCIES

Given the fact that the HR and LR states are essentially determined by the areas associated to the OV transferred in the RESET and SET transitions respectively, an interesting and quite unexplored aspect is related to the sensitivity of these processes to the peculiarities of the voltage protocol. Along this goal, in this section we analyse the associated dynamics of OV for different applied stimulus. We concentrate in the RESET process that take place for positive stimulus  $V(t)$ , but the same analysis can be performed for the SET process.

The starting point is the initial OV configuration, which is shown in both top panels of Fig.3 labeled by  $V=0$ . This OV distribution defines an initial area  $al_0$  on the left side of the interface, which we recall corresponds to the  $TiO_x$  layer. To analyse the time evolution of this initial OV density profile, we consider two positive voltage excursions (ramp1 and ramp2) of a linear ramp  $0 < V \leq V_{m1}$ , with  $V_{m1} = 900$  a.u., which differ in the rising time  $T_i$  ( $T_1 = 10$  a.u and  $T_2 = 225$  a.u.), respectively.

We focus on the evolution of the OV for the 2nd volt-

age cycle, to avoid the analysis of the initial transient in the OV dynamics, which as we have already described, manifests in an erratic behaviour of the 1st HSL (indeed observed in the experiments).

In the top panels of Fig.3, we show snapshots of the density profiles for different values of the voltages which are selected to sample the evolutions. The associated transferred areas  $a^+(V)$  are shown in the lower panels, respectively.

An important outcome is that the duration of the ramp  $T_i$  turns out to be a knob that controls whether the transfer of OV is complete or not. Notice that for ramp 1, the transferred area seems to saturate in a value  $a_{sat}^+ \sim 0.035 < al_0 = 0.05$ , before the completion of the voltage excursion.

This implies that voltage amplitudes larger than  $V \sim 600$  have not effect in transferring OV from the left to the right side of the interface. In addition, a finite amount of OV remains in the  $TiO_x$  region, consistently with the fact that the complet transfer is not achieved.

On the other hand, for the ramp 2 (right top panel of Fig.3) the initial area is fully transferred, i.e.  $a_{sat}^+ = al_0 = 0.05$ . Indeed this is attained for voltage values lower than  $V_{m1}$  (in the present case for  $V = 350$ , see the OV profile in the right top panel).

From the plateau in each plot of  $a^+$  (lower panels) we can define a saturated area value,  $a_{sat}^+$ . Doing this we have a plausible criteria to estimate the reset voltage  $V_R$ , as the voltage obtained at the intersection between the horizontal line correspondent to null transfer area with the tangent line at the value  $a_{sat}^+/2$ . This is explicitly sketched in both lower panels of Fig.3. The obtained values of  $V_R$  are in excellent agreement with the ones extracted from the HSL in the VEOV model simulations.

In the present example the complete transfer of OV is attained for ramp 2, with  $T_2 > T_1$ . We therefore can conclude that, **for linear continous ramps**, lower slopes favour the complete transfer of OV from the left to right side of the interface, once the amplitude of the ramp  $V_{m1}$  exceeds a critial voltage necessary to activate the transfer. From the above analysis the onset of the RESET transition is clearly identified with the “first arrival” of the OV front to the right hand side of the interface ( $LCMO_{3-x}$ ).

Next, we analyze the case of RESET process driven by pulsed voltage ramps, which consist in a series of pulses of increasing amplitude and time width  $\Delta T$ . Consecutive pulses are separated by  $\Delta T$  intervals with no applied voltage, as it is shown in the inset of Fig. 4 b). This type of voltage protocol is extensively used in the RS experiments.

We systematically vary  $\Delta T$ , leaving the total duration of the ramp constant. In this way, shorter  $\Delta T$  are associated with ramps with higher number of pulses. Figures 4(a) and (b) display the corresponding R vs time and R vs V associated to the RESET process, for different  $\Delta T$  shown in the legend.

We recall that larger transferred area  $a^+(V)$  implies

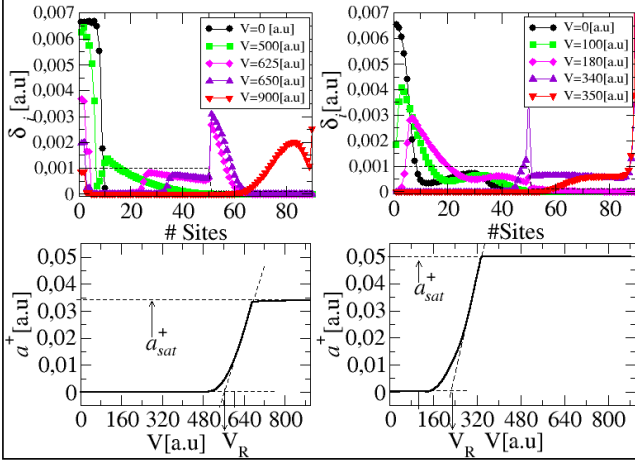


FIG. 3: Top panels: Snapshots of the OV density profile along the interface for different values of the applied stimulus  $V(t)$ , according to two protocols ramp1 (left panel) and ramp2 (right panel), defining a linear ramp  $0 < V \leq V_{m1}$ , with  $V_{m1} = 900$  a.u. and rising time  $T_1 = 10$  a.u. (ramp1) and  $T_2 = 225$  a.u. (ramp2), respectively. In dashed black line is the initial OV profile for  $t = 0, V = 0$ , which gives an area  $a_{l0} = 0.05$ . Lower panels: transferred area  $a^+$  for different voltage values shown in the upper panels legend. The RESET voltages  $V_R$  are estimated following the criteria explained in the text.

larger remnant resistance as we deduced in Eq.(5). As it can be observed from the figure, the transferred area is maximized for the shortest pulses, indicating that the OFF/ON (HR/LR) ratio is optimized by accumulating a higher amount of short pulses rather than a lower amount of wider ones. This non trivial result is experimentally confirmed for the Ti/LCMO interface, as shown in Figs 4(c) and (d), which display several RESET processes for voltage pulsed ramps with a fixed total duration of 2.88 s and different  $\Delta T$ , ranging between 2-10 ms. It is evident that a higher HR final state is achieved for shorter (2ms) pulses, confirming the prediction derived from the simulations. In addition the qualitative agreement with the numerical predictions is remarkable.

Finally, we address the study of the RESET process for trains of rectangular pulses differing in the time-widths  $\Delta T$  and amplitudes  $V_0$ , but keeping the product  $V_0 \times \Delta T = cte$ . We start by an OV profile defining an initial area  $a_{l0} = 0.05$ . The RESET process is considered as completed when the initial area is fully transferred (we choose the amplitudes  $V_0$  in order to satisfy this requirement).

The simulated evolution of  $R$  vs time, for the different trains is displayed in Fig.5(a). It is found that the number of pulses needed to achieve the RESET changes in a non-monotonic way with the amplitude  $V_0$ . This

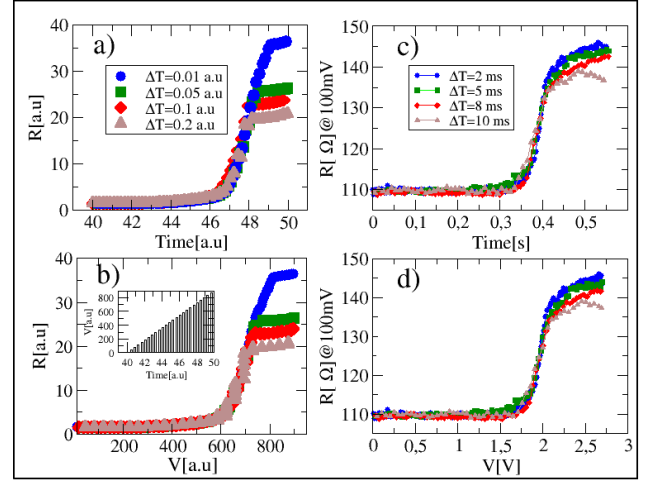


FIG. 4: Left panels: Simulations with VEOV model. a)  $R$  ( $R^+$ ) vs time and b)  $R$  ( $R^+$ ) vs  $V$ . Both plots are for a series of pulsed protocols following a linear ramp of amplitude  $V_m = 900$  a.u. but differing in the pulse duration  $\Delta T$ , as shown in the inset of panel a). A representative ramp is shown in the inset of panel b). Right panels: Experiments. c) Remnant resistance  $R$  vs time and d)  $R$  vs  $V$ , both according to different experimental protocols differing in the pulse duration.

information is indexed in Fig. 5(b), which also displays the electrical energy necessary to complete the RESET process as a function of  $V_0$  for different number of pulses labeled by the numbers. These energies were calculated as  $U = V_0^2 \sum_i \Delta T_i / R_i$ , with  $R_i$  is the attained resistance value after the application of the  $i$ -th pulse.

From this analysis we conclude that there is  $\{\Delta T, V_0\}$  pair which minimizes the RESET energy. This was indeed verified experimentally for the Ti/LCMO interface, as it is shown in Figs. 5(c) and (d). Pulse trains with  $V_0$  and  $\Delta T$  ranging between  $[1.8-3]$  V and  $[1-1.75]$  ms were tested with the product  $\Delta T \times V_0 = 3$  V ms. In the experiment we consider the RESET process as completed, when the relative resistance change after the last applied pulse is below 5%. Again, the number of pulses necessary to complete the RESET process display a non-monotonic dependence with  $V_0$ . To estimate the injected energy during each pulse, we assumed that the resistance increases linearly to its final value during the application of the pulse.

Figure 5 d) mimics remarkably well the simulated data in Fig.5 b). It is found that the RESET energy is minimized for  $\Delta T = 1.4$  ms and  $V_0 = 2.1$  V, being necessary in this case a single pulse to complete the process. For higher voltages, the RESET process can be achieved also with a single pulse but higher energy is required. For lower voltages, it is necessary to accumulate several pulses and therefore the final energy increases.

The present analysis clearly shows that the VEOV simulations appear as a powerful tool to analyze oxygen vacancies dynamics in redox memristive systems and predict optimum writing protocols to increase the efficiency of practical devices.

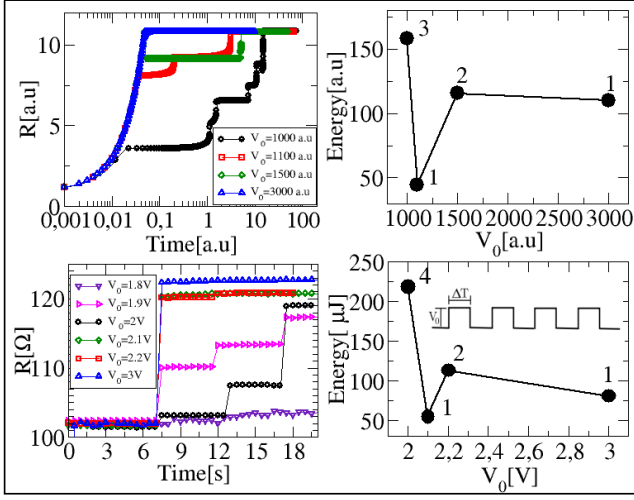


FIG. 5: Top panels: Simulations. a)  $R$  vs time for different trains of rectangular pulses satisfying  $V_0 \times \Delta T = cte$ . See text for details. b) Electrical energy injected into the system for a complete RESET process. Lower panels: Experiment: c)  $R$  vs time for different trains of pulses indicated in the legend. d) Electrical energy injected into the system for a complete RESET process. Panels b) and d) have indexed the number of pulses needed for a complete RESET.

## V. CONCLUSIONS

In summary, we have thoroughly addressed the OV dynamics in redox p-n interfaces by using an updated version of the VEOV model. The simulations allow to predict the optimum write protocols to control and enlarge the ON/OFF ratio. Our results are relevant not only for memories optimization, but also for neuromorphic computing applications, as the presence of multilevel resistance states allows mimicking the adaptable synaptic weight of brain synapses<sup>27</sup>.

In addition we found the optimum stimuli protocol that minimizes the energy consumption linked to the RESET process. This is also important for the optimization of neuromorphic computing devices aiming to emulate the highly efficient energy consumption of biological systems<sup>28</sup>.

The numerical predictions were fully validated with experiments on the Ti/LCMO memristive interface, demonstrating the power of this type of phenomenological modelling to predict and optimize the behavior of practical memristive devices.

- <sup>1</sup> J. Borghetti et al., Nature 464, 873 (2010).
- <sup>2</sup> S. Yu, Neuro-inspired computing using resistive synaptic devices, Springer International Publishing (2017).
- <sup>3</sup> G. I. Meijer, Science **319**, 1625 (2008).
- <sup>4</sup> A. Sawa, Materials Today **11**, 28 (2008).
- <sup>5</sup> R. Waser, R. Dittmann, G. Staikov and K. Szot, Adv. Mater **21**, 2632 (2009).
- <sup>6</sup> S.Q. Liu, N. J. Wu, and A. Ignatiev, Appl. Phys. Lett. **76**, 2749 (2000).
- <sup>7</sup> LCMO (PCMO) is the shorthand notation for  $La_{1/3}Ca_{2/3}MnO_3(Pr_{0.48}Ca_{0.52}MnO_3)$ .
- <sup>8</sup> J. J. Yang, I. H. Inoue, T. Mikolajick and C. S. Hwang, MRS Bulletin **37**, 131 (2012).
- <sup>9</sup> A. Herpers, C. Lenser, C. Park, F. Offi, F. Borgatti, G. Panaccione, S. Menzel, R. Waser and R. Dittmann, Adv. Mat. **26**, 2730 (2014).
- <sup>10</sup> H-S Lee, G. Y. Yeom and H-H Park, J. Phys. D: Appl. Phys. **48**, 465309 (2015).
- <sup>11</sup> A. Herpers, Electrical characterization of manganite and titanate structures, PhD Thesis, Forschungszentrum Jülich (2014).
- <sup>12</sup> F. Hossein-Babaei and S.Rahbarpour, Solid-State Electronics **56**, 185 (2011).
- <sup>13</sup> W. Román Acevedo et al., J. Phys. D: Appl. Phys. **51**, 125304(2018).
- <sup>14</sup> M. J. Rozenberg, M. J. Sánchez, R. Weht, C. Acha, F. Gomez-Marlasca and P. Levy, Phys. Rev. B **81**, 115101 (2010).
- <sup>15</sup> N. Ghenzi, M. J. Sánchez and P. Levy, J. Phys. D: Appl. Phys. **46**, 415101 (2013).
- <sup>16</sup> N. Ghenzi, M. J. Sánchez, F. G. Marlasca, P. Levy and M. J. Rozenberg, J. Appl. Phys. **107**, 093719 (2010).
- <sup>17</sup> F. G. Marlasca, N. Ghenzi, P. Stoliar, M. J. Sánchez, M. J. Rozenberg, A. G. Leyva and P. Levy, Appl. Phys. Lett. **98**, 123502 (2011).
- <sup>18</sup> N. Ghenzi, M. J. Sánchez, M. J. Rozenberg, P. Stoliar, F. G. Marlasca, D. Rubi and P. Levy, J. Appl. Phys. **111**, 084512 (2012).
- <sup>19</sup> D. Rubi, F. Tesler, I. Alposta, A. Kalstein, N. Ghenzi, F. Gomez-Marlasca, M. Rozenberg and P. Levy, App. Phys. Lett.**103** 163506 (2013).
- <sup>20</sup> Y.-F Wang et al., Sci. Rep. **5**, 10150 (2015).
- <sup>21</sup> S. Tang et al., Phys. Rev. X **6**, 011028(2016).
- <sup>22</sup> A. Asamitsu et al., Nature **388**, 50 (1997).
- <sup>23</sup> S. Menzel, M. Waters, A. Marchewka, U. Böttger, R. Dittmann, and R. Waser, Adv. Funct. Mater. **21**, 4487

- (2011).
- <sup>24</sup> J. H. Jang et al., ACS nano **11**, 6942, (2017).
- <sup>25</sup> S. Bao et al., ACS Appl. Mater. Interfaces **10** 5107 (2018).
- <sup>26</sup> T. Nagata, M. Haemori, Y. Yamashita, H. Yoshikawa, Y. Iwashita, K. Kobayashi and T. Chikyow, Appl. Phys. Lett. **99**, 223517 (2011).
- <sup>27</sup> D. Kuzum et al., Nanotechnology **24**, 382001 (2013).
- <sup>28</sup> P.A. Merolla et al., Science **345**, 668 (2014).

## ACKNOWLEDGMENTS

We acknowledge support from CNEA, UNCuyo (06/C455) and ANPCyT (PICT2014-1382, PICT2016-0867). We acknowledge L. Hueso who allowed accessing the nanoGUNE nanofabrication facilities and P. Levy for supporting this collaboration.

## Appendix A: Analytical estimates for the transferred areas

In this Appendix we derive the expressions for the transferred area  $a_k^+$  from the left to the right side of the interface, in terms of the linear and nonlinear contributions, Eq.(8).

We start by defining the rate of OV variation between neighbours sites  $i - 1$ ,  $i$  and  $i + 1$  as:

$$\Delta_i(k) = (p_{i-1,i}(k) + p_{i+1,i}(k)) - (p_{i,i-1}(k) + p_{i,i+1}(k)), \quad (\text{A1})$$

with

$$p_{i,j}(k) = C_i \delta_i(k) (1 - \delta_j(k)) \exp(I(k) \rho_i(k)) \quad (\text{A2})$$

and  $C_i = \exp(-V_\alpha)$ , already introduced in Sec. II of the main text. In the following we consider  $C_{Nl} = \exp(-V_A)$  and  $C_{Nl+1} = \exp(-V_B)$ .

Employing Eq.(A1), we write the transferred area (total number of transferred OV)  $a_k^+$  as:

$$\begin{aligned} a_k^+ &\equiv \sum_{i=Nl+1}^N \Delta_i(k) = \sum_{i=Nl+1}^N \Delta_i^L(k) + \sum_{i=Nl+1}^N \Delta_i^{NL}(k) = \\ &= a_k^{+L} + a_k^{+NL}, \end{aligned} \quad (\text{A3})$$

where we have defined:

$$\begin{aligned} \Delta_i^L(k) &= C_{i-1} \delta_{i-1}(k) \exp(I(k) \rho_{i-1}) + \\ &+ C_{i+1} \delta_{i+1}(k) \exp(-I(k) \rho_{i+1}) - \\ &- C_i [\delta_i(k) \exp(-I(k) \rho_i) + \delta_i(k) \exp(I(k) \rho_i)] \end{aligned} \quad (\text{A4})$$

and

$$\begin{aligned} \Delta_i^{NL}(k) &= -C_{i-1} \delta_{i-1}(k) \delta_i \exp(I(k) \rho_{i-1}) - \\ &- C_{i+1} \delta_{i+1}(k) \delta_i(k) \exp(-I(k) \rho_{i+1}) \\ &+ C_i [\delta_i(k) \delta_{i-1}(k) \exp(-I(k) \rho_i) + \\ &+ \delta_i(k) \delta_{i+1}(k) \exp(I(k) \rho_i)]. \end{aligned} \quad (\text{A5})$$

Performing the summations in Eq.(A3) and accounting for the boundary condition  $C_{N+1} = 0$ , we get

$$\begin{aligned} \sum_{i=Nl+1}^N \Delta_i^L(k) &= C_{Nl} \delta_{Nl}(k) \exp(I(k) \rho_{Nl}) - \\ &- C_{Nl+1} \delta_{Nl+1}(k) \exp(-I(k) \rho_{Nl+1}) \end{aligned} \quad (\text{A6})$$

and

$$\begin{aligned} \sum_{i=Nl+1}^N \Delta_i^{NL}(k) &= -\delta_{Nl}(k) \delta_{Nl+1}(k) (C_{Nl} \exp(I(k) \rho_{Nl}) - \\ &- C_{Nl+1} \exp(-I(k) \rho_{Nl+1})). \end{aligned} \quad (\text{A7})$$

The linear term  $a_k^{+L}$  has been written as the sum of two contributions,

$$a_k^{+L} \equiv P(k) - Q(k), \quad (\text{A8})$$

defined as:

$$\begin{aligned} P(k) &= C_{Nl} \delta_{Nl}(k) \exp(I(k) \rho_{Nl}(k)), \\ Q(k) &= C_{Nl+1} \delta_{Nl+1}(k) \exp(-I(k) \rho_{Nl+1}(k)). \end{aligned} \quad (\text{A9})$$

Analogously, we write the nonlinear term as:

$$a_k^{+NL} \equiv S(k) - T(k), \quad (\text{A10})$$

with

$$\begin{aligned} S(k) &= C_{Nl+1} \delta_{Nl}(k) \delta_{Nl+1}(k) \exp(-I(k) \rho_{Nl+1}(k)), \\ T(k) &= C_{Nl} \delta_{Nl}(k) \delta_{Nl+1}(k) \exp(I(k) \rho_{Nl}(k)). \end{aligned} \quad (\text{A11})$$



Notice that for current controlled experiments in which the current  $I(k)$  is known by input, the transferred areas at each time interval  $t_k$  only depend on OV densities and resistivities at the sites  $Nl$  and  $Nl + 1$ , respectively.

As we already mentioned in Sec. II, the activation energies for OV diffusion satisfy  $V_A < V_B$  and thus  $C_{Nl+1} < C_{Nl}$ . Therefore, we can safely approximate:

$$a_k^+ = a_k^{+L} + a_k^{+NL} \approx P(k) - T(k). \quad (\text{A12})$$

This equation can be updated for the next time interval  $t_{k+1}$  employing

$$\delta_i(k+1) = \delta_i(k) + \Delta_i(k), \quad (\text{A13})$$

for  $i = Nl - 1, Nl$  and  $Nl + 1$ , respectively.

From Eq. (A2) and Eq. (A1) we write after a straightforward algebra:

$$\begin{aligned} \Delta_{Nl}(k) = & C_{Nl} \delta_{Nl}(k) [-2 \cosh(I(k) \rho_l(k)) + \\ & + \delta_{Nl+1}(k) \exp(I(k) \rho_{Nl}(k)) + \\ & + \delta_{Nl-1}(k) \exp(-I(k) \rho_{Nl}(k))] + \\ & + (1 - \delta_{Nl}(k)) \\ & [C_{Nl+1} \delta_{Nl+1}(k) \exp(-I(k) \rho_{Nl+1}(k)) + \\ & + C_{Nl-1} \delta_{Nl-1}(k) \exp(I(k) \rho_{Nl-1}(k))]. \end{aligned} \quad (\text{A14})$$

Performing the substitution  $k \rightarrow k + 1$ , replacing Eq. (A13) in  $P(k)$  (Eq. (A9)), and taking into account Eq. (1) in the main text, we obtain:

$$\begin{aligned} P(k+1) = & C_{Nl} [\delta_{Nl}(k) + \Delta_{Nl}(k)] \\ & \exp(I(k+1)(\rho_0^l - A(\delta_{Nl}(k) + \Delta_{Nl}(k))). \end{aligned} \quad (\text{A15})$$

In a similar way we derive, after updating  $T(k)$  in Eq. (A11),

$$\begin{aligned} T(k+1) = & C_{Nl} [\delta_{Nl}(k) + \Delta_{Nl}(k)] [(\delta_{Nl+1}(k) + \Delta_{Nl+1}(k)) \\ & \exp(I(k+1)(\rho_0^l - A(\delta_{Nl}(k) + \Delta_{Nl}(k)))]. \end{aligned} \quad (\text{A16})$$

Employing these two last equations we compute  $a_{k+1}^+ \approx P(k+1) - T(k+1)$ .

Following the described prescription iteratively, the total transferred area  $a^+$  after an elapsed time  $t_+ = \sum_k t_k$ , can be computed under the present assumptions.

The same procedure can be applied to compute  $a^-$  for negative electrical stimulus. Assuming that the current protocol  $0 \rightarrow I_{m1} \rightarrow 0$  is completed for a time  $T_+ = \sum_k^{K^+} t_k$ , the initial condition for the negative current protocol  $0 \rightarrow -I_{m2} \rightarrow 0$  should be taken as the OV profile at time  $T_+$ , i.e.  $\delta_i(K_+)$ .

To avoid repetition we give below the final expression, valid for  $k > K_+$ :

$$\begin{aligned} a_k^- = & C_{Nl} \delta_{Nl}(k) \exp(I(k) \rho_{Nl}) - \\ & - C_{Nl+1} \delta_{Nl+1}(k) \exp(-I(k) \rho_{Nl+1}) + \\ & + \delta_{Nl}(k) \delta_{Nl+1}(k) (C_{Nl+1} \exp(-I(k) \rho_{Nl+1}) - \\ & - C_{Nl} \exp(I(k) \rho_{Nl})). \end{aligned} \quad (\text{A17})$$